Magnetic tweezers for DNA micromanipulation

Charbel Haber[a)]
Department of Chemical Engineering, The Johns Hopkins University, 3400 N. Charles St., Baltimore, Maryland 21218

Denis Wirtz[b)]
Department of Chemical Engineering and Department of Materials Science and Engineering, The Johns Hopkins University, 3400 N. Charles St. Baltimore, Maryland 21218

(Received 24 July 2000; accepted for publication 19 September 2000)

We detail the design of an electromagnetic assembly capable of generating a constant magnetic field superimposed to a large magnetic field gradient (between 40 and 100 T/m), which was uniform over a large gap (between 1.5 and 2 cm). Large gaps allowed the use of wide high numerical-aperture lenses to track microspheres attached to DNA molecules with an inverted light microscope. Given the geometric constraints of the microscope, computer-aided design was used to optimize the magnetic field gradient linearity, homogeneity, and amplitude, as well as the arrangement of the magnetic coils, the currents, and the mechanical stability of the assembly. The assembly was used to apply forces of controlled amplitude, direction, and time dependence on superparamagnetic microspheres by using magnetic coils instead of permanent magnets. A streptavidin-coated microsphere was attached to the 3′ end of a λ-phage DNA molecule through a single biotin molecule. The 5′ end of the λ-phage DNA molecule was tethered to a glass coverslip by conjugating the DNA's overhang to a complementary 12 base-pair primer, which was itself cross-linked to a heterobifunctional group placed on the glass coverslip. By tracking the centroid of this microsphere, the mechanical response of a single λ-phage DNA molecule was measured as a function of the applied magnetic force. The resulting force-extension curve was fitted with the worm-like-chain model to obtain λ-phage DNA's persistence length and contour length, which were in agreement with previous reports. © *2000 American Institute of Physics.*
[S0034-6748(00)05212-6]

I. INTRODUCTION

Fifty years ago, Crick and Hughes probed the physical properties of the cytoplasm of adherent cells using micron-sized magnetic particles and permanent magnets as ''magnetic tweezers.'' [1] Crick and Hughes realized that magnetic tweezers offered a low-cost, versatile tool to characterize the physical properties of complex systems such as living cells. Recently, magnetic tweezers have been used to measure the micromechanical and transport properties of individual DNA molecules as well as the force produced by individual motor proteins.[2–8] Magnetic tweezers have also been utilized to demonstrate mechanotransduction through the cellular plasma membrane and to measure the micromechanics of cytoskeleton networks *in vitro* and *in vivo*.[9–18]

Magnetic tweezers implicate a force, which is generated by a magnetic field gradient that can be controlled using different types of assemblies. For instance, in conjunction with a flow field, Smith, Finzi, and Bustamante[2] recently utilized two movable permanent magnets that induced a lateral force on magnetic beads to stretch individual DNA molecules. Strick *et al.*[5,19] also used permanent magnets to control the amount of twisting on a magnetic bead connected to a DNA molecule, and studied DNA supercoiling. Sackmann and co-workers[10,18,20] substituted the permanent magnets for magnetic coils containing cylindrical soft-iron cores to map the mechanical properties of *F*-actin networks *in vitro* and the cytoskeleton of live cells. Wang, Britler, and Ingber[9] demonstrated mechanotransduction across the cell membrane and through the cytoskeleton of live cells by twisting nanospheres coated with cell-receptor antibodies or ligands. Most of the above magnetic manipulators show some advantages over optical tweezers as they eliminate possible damages to the samples due to localized heating.[21]

Magnetic coils offer the salient advantage over permanent magnets to generate magnetic fields and magnetic-field gradients, which can be more easily controlled. Literature pertaining to nuclear magnetic resonance instrumentation provides a wealth of information on how to design magnetic-field gradient coils.[22] One practical method that makes use of electromagnets requires capping the protruding poles with parabolic surfaces, which are machined so that their first derivative with respect to the separating distance is linear. Alternative methods which achieve a good linearity consist of varying the shapes of coils.[23] Another popular configuration involves Maxwell coils, which consist of two flat circular wire coils oriented parallel and coaxial to each other, and additional coil loops used to provide a greater degree of linearity.[24] Amblard *et al.*[11,13] built an apparatus that ma-

[a)]Current address: Merck Research Laboratories, P.O. Box 4, West Point, PA 19486.
[b)]Author to whom all correspondence should be addressed; electronic mail: wirtz@jhu.edu

nipulated magnetic beads via four independent magnetic elements placed normal to the optical axis of a light microscope to measure the rheological properties of actin gels. To generate a gradient field, a large magnetic field was applied at one pole, while the field of the other three coils was held at a value approximately one-third of the first coil.[11] A disadvantage of that instrument for applications such as single-molecule manipulation is that it can only produce forces that are (typically) less than 0.1 pN for a gap of 1 cm.[11]

Most of the above systems are either too voluminous for a microscope (and associated geometric constraints), or the magnetic-gradient field that they produce is not high enough to generate large forces over a large gap. This article reports the practical knowledge needed to design magnetic tweezers, which can be conveniently placed on the stage of a commercial microscope and can generate large and highly linear magnetic-field gradients over relatively large distances. Using computer-aided design (CAD) tools, we optimized the arrangement and materials used for the magnetic manipulators. Working at maximum capacity, our magnetic tweezers generated a uniform gradient of $\approx$40 T/m for a gap of 2 cm or $\approx$100 T/m for a gap of 1.5 cm. These magnetic field gradients were significantly higher than provided by assemblies presented in the literature, especially for such large gaps. Our instrument could be employed in conjunction with wide microscope lenses (such as high-numerical aperture oil-immersion or water-immersion lenses) and could control the amplitude, direction, and time dependence of the force field acting on magnetic beads by using magnetic coils instead of permanent magnets.

II. THEORY

We briefly derive the conditions for applying a constant force on a superparamagnetic bead. The potential of a magnetic dipole moment **m** in a constant magnetic field **B** is given by $U=-\mathbf{m}.\mathbf{B}$. The corresponding magnetic force is the gradient of the potential U

$$\mathbf{F}=\nabla(\mathbf{m}.\mathbf{B}). \tag{1}$$

The induced magnetic moment has the same direction as the magnetic field flux, **B**, therefore, in the following, the bold vectorial notation is dropped because only one direction is considered. For large magnetic fields and because of the inherent properties of superparamagnetic microspheres, the magnetization saturates within the magnetic bead and M approaches a magnetic field-independent value $M_{\max}$, which corresponds to the complete alignment of all the magnetic dipoles contained in the volume V of the bead. In that case, the dipole moment, $m=MV$, becomes independent of the applied field and Eq. (1) becomes

$$F\approx M_{\max}VdB/dx. \tag{2}$$

Therefore, two fields have to be applied to produce a constant force: a homogeneous magnetic field, which must be large and uniform so that the bead magnetization is constant ($M\approx M_{\max}$), and a constant magnetic-field gradient dB/dx, so that the force on the superparamagnetic bead is constant.

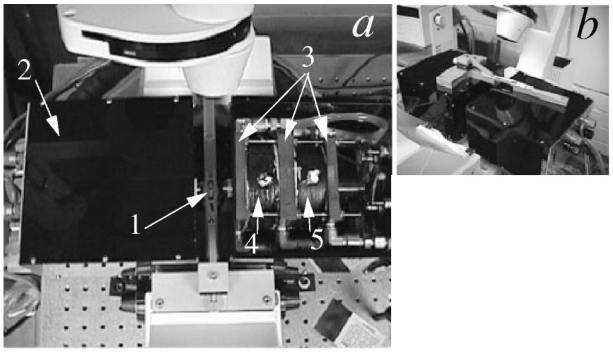

FIG. 1. Setup used to apply a homogenous magnetic field superimposed to a magnetic-gradient field. (a) Two circular identical coaxial coils are used with a separation equal to the turn of the radius and with current flowing in the same direction in each coil. Arrows indicate: (1) the thin aluminum mount used to contain the DNA specimen; (2) one of the two sets of homogenous + gradient coils; in operating mode, both sets are contained in plastic boxes; (3) three water-cooling jackets are used to evacuate the heat generated by the coils; (4) the gradient coil and (5) the homogeneous coil. A thermally conductive material is used in the assembly of the magnetic windings and an electrically insulating and thermally conductive layer is spread between both the coils and the water-cooling jackets to minimize the presence of air spaces. (b) The magnetic tweezers are mounted on an inverted microscope, which is itself mounted on an optical table for stability.

III. METHODS AND MATERIALS

A. General overview

The 3′ end of a λ-phage DNA molecule was attached to a superparamagnetic bead via a streptavidin/biotin link (see Secs. III C and III G). Simultaneously, the 5′ end of the DNA molecule was attached to a glass coverslip through a primer complementary to the overhang of the DNA molecule (see Secs. III D–III F). Magnetic tweezers mounted on an inverted light microscope and composed of two sets of coaxial electromagnetic coils (see Sec. III B) rendered the magnetization of the bead constant (see Sec. II) and generated a uniform force (see Secs. III H and III J). Video-enhanced particle-tracking microscopy monitored the displacements of the bead in the presence of the applied magnetic force (see Sec. III I). Finally, force-extension curves of individual DNA molecules were generated, from which both the persistence length and the contour length of λ-phage DNA were extracted (see Sec. IV).

B. Design and optimization of magnetic tweezers

Since the probe microspheres used here are paramagnetic, the magnetic field within the field of view of the microscope cannot vanish. Indeed, if the field vanished, the magnetization of the bead, the bead's magnetic moment and the applied force would vanish as well [see Eq. (1)]. To obtain a nonzero, uniform force over a large viewing area perpendicular to the optical axis of the microscope, a homogeneous magnetic field was superimposed to a magnetic-gradient field (Fig. 1). To change the magnitude of the force, the gradient field was displaced upward or downward by the homogeneous field. To reverse the direction of the force, the polarity of the homogeneous field (i.e., the current direction in the homogeneous coils) was inverted. A relatively wide region of uniform and controllable magnetic fields and

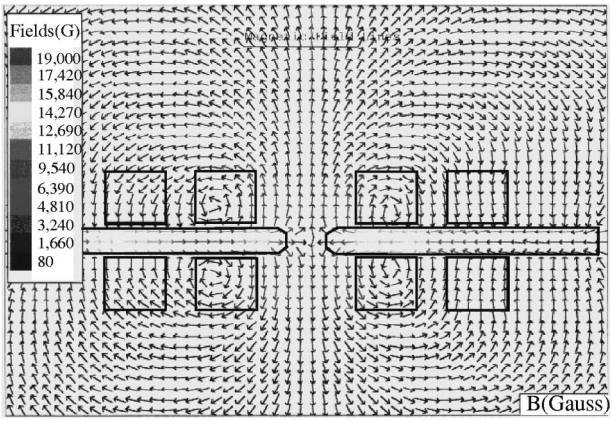

FIG. 2. Simulated magnetic-field distribution (contour maps) obtained with the design software Magneto (Manitoba, Canada). The currents for the homogenous field set of coils and the gradient set of coils are 5000 A turns and 25 000 A turns, respectively. This type of simulation helped us optimize the currents, coil size and separation, and the core materials of the magnetic tweezers.

magnetic-field gradients was produced by two sets of coaxial Helmholtz coils. For each set, two circular identical coaxial coils were separated by a distance equal to the turn of the radius and used with currents flowing in the same direction in each coil (Fig. 1).

The magnetic field contribution at any point from a circular coil, $d\mathbf{H}$, due to a current element $I\mathbf{dl}$, is given by

$$d\mathbf{H}=(I\mathbf{dl}\times\mathbf{u})/4\pi r^2, \tag{3}$$

where r is the distance from the coil along its axis, I is the current in the coil, and $\mathbf{u}$ is a unit vector along the radial direction. To find off-axis components of the magnetic field H, we integrated Eq. (3) using a boundary-element numerical approach developed by Integrated Engineering Software Magneto (Manitoba, Canada) (Figs. 2 and 3). This software allowed us to simulate various geometries with their specific material properties, boundary conditions, and currents to optimize the force applied on a microsphere given the geometric constraints of the microscope.

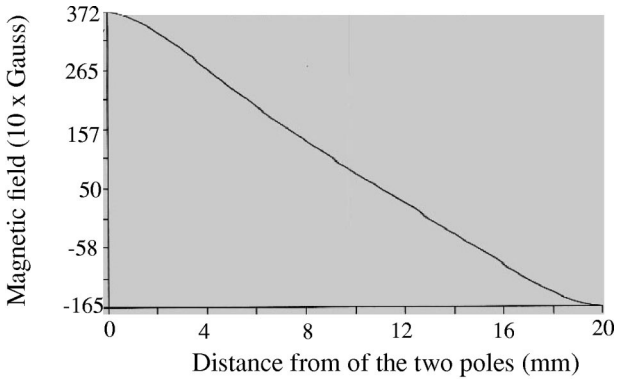

FIG. 3. Predicted magnetic-field strength between the poles of the magnetic tweezers as a function of the separation distance between the poles. The currents for the homogenous field set of coils and the gradient set of coils are the same as in Fig. 2. This magnetic field was calculated by using the design software Magneto.

1. Type of wires for the magnetic coils

The coils used here to produce a homogeneous magnetic field and magnetic field gradient were made of conducting metal; two metal conductors were considered, copper and aluminum. In our case, the density of copper (3.2 times that of aluminum) and its conductivity (60% higher than aluminum) made copper a more suitable material. Higher density provided extra weight which stabilized the magnetic-tweezers assembly; higher conductivity helped remove heat generated at high currents more efficiently. To produce forces of adequate magnitude, the gradient and homogeneous coils were assigned 25 000 A turns and 5000 A turns, respectively (see more below). The diameter of the wires was selected according to the number of ampere turns of the gradient and homogeneous coils, the generated heat, the capacity of the available power supplies, and the amplitude of the forces to be generated. We used the American Wire Gauge (Allied Electronics Data Handbook, Fort Worth, TX), which lists copper wires of different diameters and resistivities at various temperature. Wire characteristics were matched to the current/voltage of our power supplies, a Sorensen DCR-600-16 T1 0116 rated to 700 and 16 A and a Kepco BOP 72-6M bipolar operational power supply/amplifier rated to 72 V and 6 A, (Kepco, Korea). We selected No. 18 for the homogeneous set of coils (Cotronics, Brooklyn, NY), generating a maximum of 5000 A turns, which require a power consisting of 5.8 A in current and 62 V in voltage. We chose No. 21 for the gradient set of coils (Cotronics) generating 25 000 A turns, which necessitated a power supply that accommodated a current of 14.5 A and a voltage of 620 V. Electric connections between coils, power supplies, and function generator are described in Fig. 5.

2. Material for the cores placed inside the magnetic coils

To further augment the range of applied forces, soft-iron cores were placed inside the Helmoltz coils (Figs. 1 and 4). The cores were made of an iron–vanadium–cobalt soft alloy (Hiperco Alloy 50 A, Scientific Alloys, Inc., Westerly, RI), which possesses a very small hysteresis and a high magnetic saturation of 24 kG. When the cores were inserted inside the coils, the induced field B was enhanced by an additional contribution $4\pi M$, $B=H+4\pi M$, where M is the magnetization of the material. The metal cores in each set of coils also brought the magnetic field closer to the specimen (Fig. 4).

3. Geometry of the magnetic coils

The space available for the magnetic coils was limited by both the length of the microscope objective (100× magnification, 1.4 numerical aperture, water-immersion lens, Carl Zeiss, Germany), which is ≈4 cm, and the maximum height allowed by the microscope's condenser (Axiovert 100, Carl Zeiss), which is ≈5 cm above the objective (see Fig. 1). On that basis, the outer diameter of the coils was chosen to be 8 cm (Fig. 4).

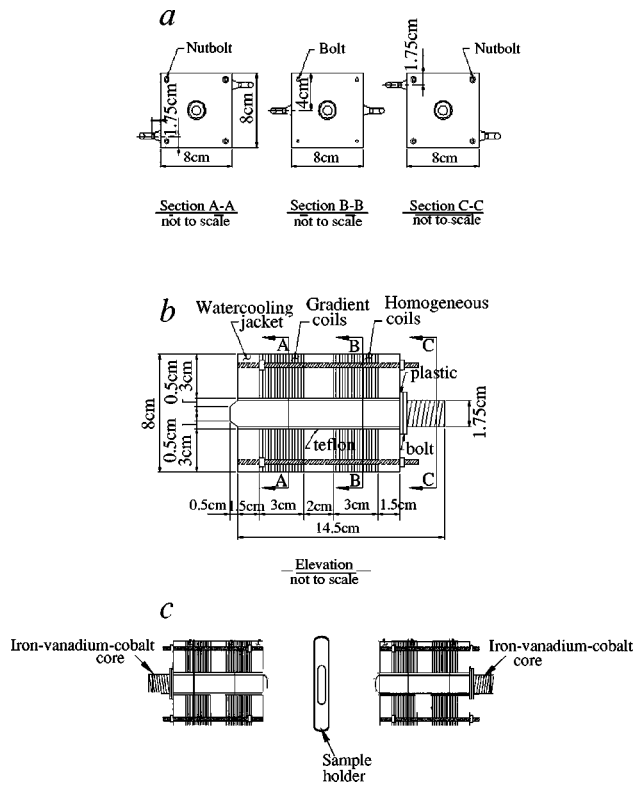

FIG. 4. Design of the magnetic-tweezer assembly and the water-cooling jackets to minimize the heat generated by the tweezers. (a) Front, middle, and back of the water-cooling jackets. Three water-cooling jackets are used per set of homogenous + gradient coils. (b) Detailed computer-aided design (CAD) drawing of one of the two sets of coils for the magnetic tweezers. (c) Assembly and orientation of the two sets of homogenous + gradient coils.

The homogeneity of the magnetic field and magnetic-field gradient depends on the characteristics of the magnetic poles of the assembly, such as their shape, the type and texture of the magnetic material, and the ratio of pole-face diameter to gap width. Using the software Magneto, the positions of the homogeneous and gradient coils were varied to optimize gradient linearity and homogeneity. The boundaries (i.e., the edges of the magnets) were drawn first. Then, the magnetic materials (cores and coils) were selected and placed in the appropriate regions, and assigned a current, measured in amperes turn. Information on the field distribution was obtained in the form of contour maps and field plots (Fig. 2) and the magnetic-field gradient strength between the poles was plotted as a function of the separation distance between the poles (Fig. 3). Higher gradients were generated when the homogeneous coils were placed behind the gradient coils with respect to the optical axis of the microscope (see Figs. 1 and 4). Decreasing the diameter of the coils, and therefore of the poles, increased the magnetic field flux, but reduced linearity. For improved homogeneity over the same volume, or for the same homogeneity over a large fraction of the gap width, one must increase the ratio of the pole diameter to gap width. Using Magneto, a core diameter of 1.5 cm over a gap ranging between 1.5 and 2.0 cm was found to be the best compromise between homogeneity and field strength. To achieve maximum field strength with the above setup, the pole pieces were tapered at the extremities. The free poles formed on the tapered surface contributed to the field at the center of the gap. In our instrument, the size of the air gap (distance between the poles) could be adjusted by screwing the cores in and out.

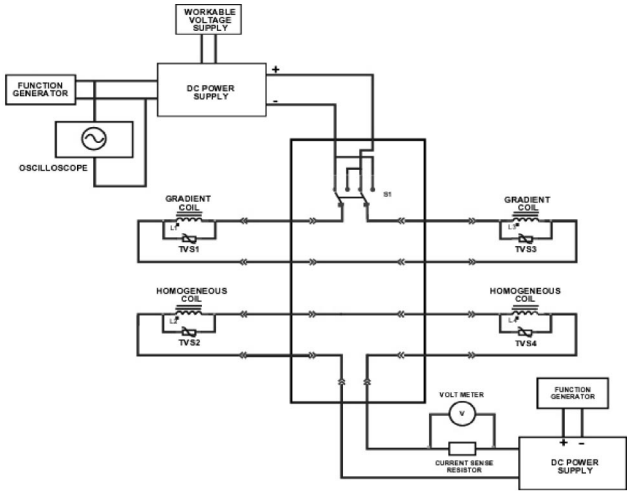

FIG. 5. Schematic diagram of the circuit board used to control the magnetic tweezers. This represents the electric connections between the coils, the power supplies, the sensors, and the function generator.

4. Safety precautions and magnet-coil cooling

Producing large magnetic fields require very high currents; therefore, removing efficiently large amounts of heat was a key issue, and was accomplished by winding the wires on water-cooled brass boxes (Figs. 1 and 4). Moreover, a thermally conductive material, Duralco 132 (Cotronics), which consisted of aluminum-filled epoxy, was used in the assembly of the magnetic windings. An electrically insulating and thermally conductive layer of Duralco 134 (Cotronics) was spread between both the coils and the water-cooling jackets to minimize the presence of air spaces (Figs. 1 and 4).

In the event of power failure or disconnection of a supply conductor, the magnetic field could decrease abruptly. This sudden change of magnetic flux can induce substantial induced voltages, causing currents to flow around the instrument, which could result in serious injury. One preventative measure adopted here was to place a diode across the inductor. When the diode's switch is on, the diode is back biased from the dc drop across the inductor's winding resistance; when the switch is off, the diode goes into conduction, putting the switch terminal a diode drop above the positive supply voltage. Transient voltage suppressers, PHP-60 and PHP-80 (Protek Devices, Tempa, AZ), were added to protect the equipment and the operators from power surges and transients originating from inductive switching or power interruption (Fig. 5). To insulate all exposed power connections inside the instrument, the poles were shielded from the electromagnetic coils using Teflon heat-shrinking tubing.

C. Microspheres for DNA manipulation

To exploit our magnetic tweezers for DNA micromanipulation, we used 2.8-μm-diam, superparamagnetic microspheres (M280, Dynal, Norway), which were coated with streptavidin, a protein made up of four identical subunits

each containing a high affinity binding site for biotin ($K_D \approx 10^{-15}$ M). The biotin–streptavidin bond, which was used here to attach DNA to the microsphere, is one of the strongest known noncovalent bonds and is stable over a wide range of temperatures and pH levels. Dynal beads M-280 have a saturated magnetic moment of 1.42×10^{-13} Am^2 (Dynal).

D. DNA preparation

1. λ-phage DNA

For DNA micromanipulation, we used λ-phage DNA, which is isolated from the bacteriophage λ (c1857*ind* 1 *Sam* 7) of *E-coli*, and is one of the best characterized DNA molecules.[25] In circular form, λ-phage DNA contains 48 502 base pairs, its molecular weight is approximately 3.15×10^7 Da, and its contour length is $\approx$16.5 μm. The λ-phage DNA was purchased from New England Biolabs (Beverly, MA) and came in a concentration of 500 μg/ml in TE buffer (10 mM Tris-HCl (pH 8.0), 1 mM EDTA). What distinguishes λ-phage DNA are its overhangs (sticky ends), which are 12 base pair (bp) long single strands.[26] These overhangs allow λ-phage DNA to easily be derivatized with various functional groups for attachment both to a glass coverslip and to a magnetic bead (see more below).

2. Biotinylation of DNA for subsequent attachment of the magnetic bead

For attachment to the streptavidin-coated magnetic microspheres, λ-phage DNA molecules were byotynalated by filling in the 3′ overhang of λ-phage DNA with a complementary primer containing a biotin molecule. This primer consisted of 12 bp forming the sequence 5′-GGG CGG CGA CCT (Biosynthesis & Sequencing Laboratory at The Johns Hopkins Medical School, Baltimore, MD). To limit multiple attachment of molecules to the bead, the DNA molecule was biotinylated by attaching a single (as opposed to several)[19] biotin molecule to the 3′ end of the primer. A solution of 10 μg/ml of λ-phage DNA (New England Biolabs) was mixed with an equimolar amount of biotinylated primers in TE buffer (10 mM Tris-Cl, 1 mM EDTA, pH 8.0). The reaction volume of 150 μl was heated to 70 °C for 10 min to linearize any circular λ-phage DNA, and was allowed to anneal at room temperature for 1 b. The λ-phage DNA concentration used here, 10 μg/ml, was smaller than the overlap concentration, $c^*\approx 40-50\,\mu$g/ml, to minimize the formation of DNA multimers.[26,27] A volume of 17 μl of 10× ligase buffer was added to the solution. Subsequently, 1.5 μl of T4 DNA ligase (New England Biolabs) was transferred to a microcentrifuge tube, which was incubated at 16 °C for 6 h. To quench the reaction, EDTA was added to the solution, which then was heated for 10 min at 60 °C to inactivate the enzyme. Biotinylated DNA was dialyzed against TE buffer using a regenerated cellulose membrane with a molecular weight cutoff of 100 kDa (Spectrum, Laguna Hill, CA). Dialyzed biotinylated DNA solutions were stored at 4 °C.

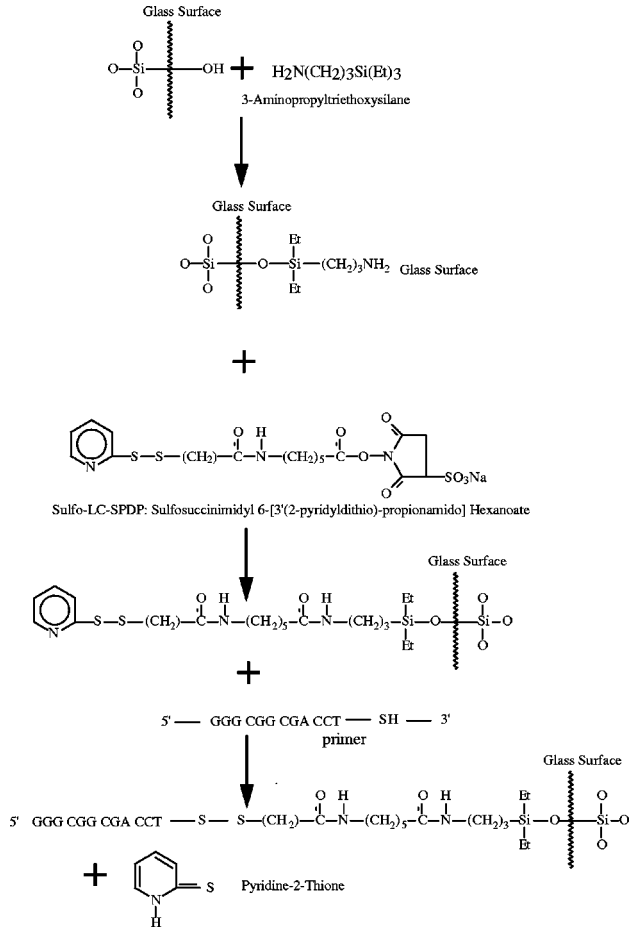

FIG. 6. Steps leading to the attachment of the sulfhydryl primer to a glass substrate. These steps consist of an acid wash of the glass substrate, followed by a silanization step using a 20% solution of TESPA and 80% HPLC grade acetone. This step is followed by the attachment of thiolated primers (5′-AGG TCG CCG CCC), which are complementary to the free overhang of the biotinylated λ-phage DNA. The sulfhydryl group (i.e., the thiol group) is attached to the C nucleotide on the 3′ end and the phosphorus group is attached to the 5′ end. Thiolated DNA primers are end tethered to the aminosilane film formed on the silica surface of the coverslip using a heterobifunctional cross-linker, sulfosuccinimidyl 6-[3′-(2-pyridyldithio)-propioamido] hexanoate (Sulfo-LC-SPDP). At this point, the modified coverslip surface consists of covalently grafted 12 bp primers that are complementary to the previously prepared biotinylated DNA. To attach DNA to the modified coverslip, biotinylated λ-phage DNA is spread on the surface of the coverslip. A ligation reaction between biotinylated DNA molecules and the coverslip is induced by ligase.

E. Surface modification

The various steps leading to the attachment of the sulfhydryl primer to a glass substrate are depicted in Fig. 6 and consisted of the following:

1. Acid wash of the glass coverslip

This first step consisted in systematically cleaning the surface of the glass coverslip (Clay Adam No. 0) by immersion in a bath of sulfuric acid and Nochromix cleaning solution (Godax Laboratories, Takoma Park, MD) for 15 min. Thorough rinsing with distilled de-ionized water (ddH_2O) followed. The coverslips were dried in an oven maintained at 100 °C.

2. Silanization of the glass coverslip

The surface of the cleaned coverslips was derivatized with a self-assembled monolayer of γ-Aminopropyltriethoxysilane (TESPA) (Pierce, Rockford, IL) (Fig. 6). This silanization step consisted in immersing the glass coverslips in a 20% solution of TESPA and 80% HPLC grade acetone (Aldrich, Milwaukee, WI) for 20 s, then rinsing them twice with acetone and once with ddH_2O to remove the excess of coupling-agent molecules. The silanized coverslips were incubated at 37 °C for 1 h.

3. Thiolated primers to be cross-linked to the silanized coverslip

Prior to cross-linking to the silanized surface of the coverslips, primers were thiolated. The sequence of the primer is 5′-AGG TCG CCG CCC (Biosynthesis & Sequencing Laboratory at The Johns Hopkins Medical School), which is complementary to the remaining free overhang of the biotinylated λ-phage DNA (see Fig. 6). The sulfhydryl group (i.e., the thiol group) was attached to the C nucleotide on the 3′ end and the phosphorus group was attached to the 5′ end. Thiol-modified primers were stored in TE buffer. The thiol group is labile and is very susceptible to oxidation or deactivation by heavy metals such as mercury, copper, or silver, which may contaminate the solutions. To protect the SH group, dithiothreitol salt (DTT, $HSCH_2(CHOH)_2CH_2SH$; Amersham Pharmacia Biotech, Piscataway, NJ) was added to the buffer containing the primer to prevent oxidative disulfide formation. DTT is smaller in size than the primer, and therefore diffuses more quickly. Moreover, DTT has two SH groups, leading to an increase in the probability of collisions with any SH predator. A solution of 50 ng/ml of SH primer was reduced with 100 mM DTT in TE solution at $p\mathrm{H}=8.4$ for 30 min at room temperature. DTT was removed on a desalting column prepacked with Sephadex G-25 (Amersham Pharmacia Biotech). Thiolated primers were added immediately to the coverslips.

4. Cross-linking of the primers to the glass coverslip

Thiolated DNA primers were cross-linked to the aminosilane film formed on the silica surface of the coverslip using a heterobifunctional cross-linker, sulfosuccinimidyl 6-[3′-(2-pyridyldithio)-propioamido] hexanoate (Sulfo-LC-SPDP; Pierce) (Fig. 6). This cross-linking approach was recently adopted by Hegner, Smith, and Bustamante.[28] The heterobifunctional, cleavable cross-linker, which contains both thiol and amino reactive moieties, reacted with the primary amines of the silane coat and the sulfhydryl groups of the DNA molecule. The cross-linker solution consisted of 3 mg of Sulfo-LC-SPDP dissolved in 1 ml of phosphate buffer saline (PBS Sigma, St. Louis, MO). The silanized coverslips were submerged for 1 h in the cross-linker solution, made immediately prior to use, then quenched in TE buffer (10 mM Tris base and 1 mM $EDTA.Na_2.2H_2O$) for 10 min.

F. DNA attachment to the primer-grafted coverslip

The modified coverslip surface consisted of covalently grafted 12 bp primers that were complementary to the previously prepared biotinylated DNA. To attach DNA to this modified coverslip, 80 μl of 0.5 μg/ml biotinylated λ-phage DNA was spread on the surface of the coverslip (Fig. 6). A ligation reaction between biotinylated DNA molecules and the coverslip was performed by adding 9 μl of 10× ligase buffer and 1 μl of ligase (20 units/μl) (New England Biolabs). In addition to creating a covalent bond between the grafted primer and the biotinylated DNA, ligase repaired accidental nicks induced by sample handling. The whole construct was incubated at 16 °C for 6 h. The ligation was terminated by addition of 15 μl of EDTA, which chelated the divalent cations. This last step has another subtle benefit: due to the presence of 10 mM of magnesium chloride in the buffer, DNA molecules adhered to the substrates due to the screening of electrostatic repulsion. After a delicate rinse with TE buffer coverslips were covered with TE buffer and stored at 4 °C. Grafted DNA molecules remained functional for 2–3 days.

G. Attachment of the magnetic bead to λ-phage DNA

Next, the streptavidin-coated, superparamagnetic beads were attached to the DNA molecules. The beads were washed once before usage by resuspending them in TE buffer, then by applying a magnetic field gradient (a permanent magnet is placed on the wall of the centrifuge tube), aspirating the supernatant composed of bovine serum albumin, NaN_3, and Tween 20 (Zymed Laboratories, South San Francisco, CA), and by resuspending the beads in TE buffer. The assembly buffer for bead attachment consisted of 100 mM NaCl to promote the reaction between biotin and streptavidin, washed magnetic beads ($\approx 3.0\times 10^6$ Dynal beads/ml), 3 mM NaN_3 to prevent the growth of microorganisms, and 0.1% Tween 20, a surfactant used to minimize nonspecific binding of the beads to the surface or to the DNA. The beads were put into contact with the tethered DNA molecules for 3–5 min; if the beads were left for a longer time in contact with the grafted coverslip, they adhered irreversibly. The reaction was stopped by flipping the glass coverslip; the unattached beads precipitated due to their high density compared with water. If a different solution composition was desired, the coverslip was rinsed very gently before addition of the new buffer solution.

H. Force calibration

The magnitude of the magnetic field produced by the magnetic tweezers was mapped between the poles using a magnetometer (Gauss/Tesla model 4048, F.W. Bell, Orlando, FL). We found that the fields were extremely homogeneous for various combinations of homogeneous and gradient fields. Figure 7 illustrates the magnetic field obtained for a homogeneous coil current of 2 A and a gradient coil current of 6 A. The magnetic forces on untethered magnetic beads, suspended in a medium containing $CaCl_2$ (25% w/v), were measured using a balance between the applied magnetic force and the resulting friction force on the beads (see also Smith and co-workers[2]). A small concentration of beads was used so that hydrodynamic interactions between beads could be neglected. The solution density was chosen to be equal to

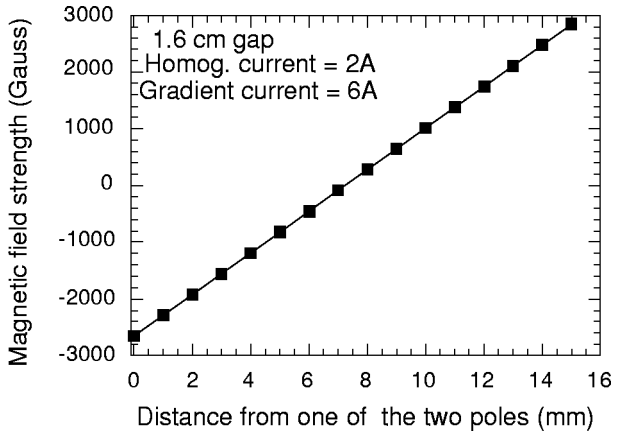

FIG. 7. Magnetic-field generated by the magnetic tweezers. The homogeneous coil current is 2 A and the gradient coil current is 6 A, currents that are typical of those used to probe DNA micromechanics. The magnetic forces on untethered magnetic beads, suspended in a medium containing $CaCl_2$ (25% w/v), are measured using a balance between the applied magnetic force and the resulting friction force on the beads.

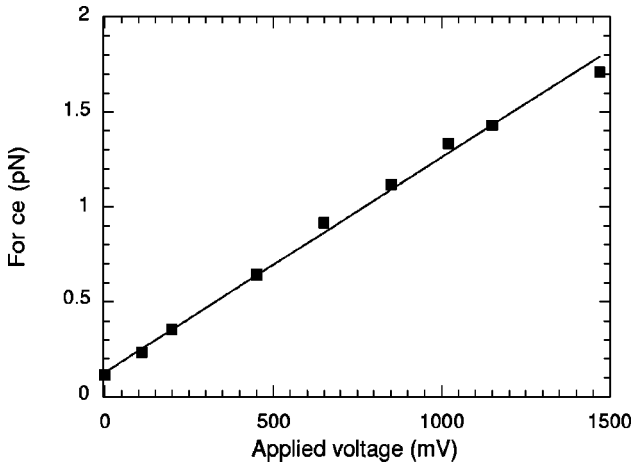

FIG. 8. Calibration curve that delineates the relationship between the voltage drop applied to the magnetic tweezers and the force experienced by the magnetic bead.

the beads' density to prevent their sedimentation. The viscosity of the medium was measured separately using a rheometer (ARES 100, Rheometrics, Inc., Piscataway, NJ) as described,[29,30] and was found to be ≈6 cP (viscosity of water ≈1 cP at 25 °C). Because the bead's velocity was on the order of μm/s, the Reynolds number did not exceed 10^{-5}. In this low Reynolds-number regime, Stokes' drag formula could be used to estimate the force applied on the magnetic bead, F_M:

$$F_M \approx 6\pi\eta a v, \tag{4}$$

where η is the viscosity of the buffer, $a = 1.40\,\mu$m is the radius of the bead, and v is the measured bead velocity. To minimize wall effects, the velocity was measured in the midplane of the cell, which is approximately 20 beads away from the surface. The bead position was determined using a particle-tracking code written with NIH Image (see section III I). The velocity of the beads was determined for various gradient fields while the homogeneous fields were kept at a constant amplitude. A calibration curve that delineated the relationship between the applied voltage drop and the force experienced by the magnetic beads was generated (Fig. 8). If necessary, to generate an oscillatory force on a magnetic bead, a sinusoidal current can be applied using the synthesized-function generator (Stanford Research Systems DS340 15 Mhz, Palo Alto, CA) or by programming a function using Lab View and feeding it to the bipolar power supply (Kepco).

I. Image processing and particle tracking

The beads were observed with bright-field light using a Zeiss Axiovert 100 microscope (Carl Zeiss), equipped with a 100× water-immersion objective. Images of the attached beads moving under the influence of the magnetic force were acquired with a solid-state charge coupled device camera (Cohu, Japan),[31] enhanced with an image processor (Argus-10), and recorded with an S-VHS VCR (JVC, Japan) as described.[32,33] Positions of the beads were monitored using a multiple-particle tracking software written in the Wirtz lab.[34] Images of microspheres were acquired with NIH Image (NIH, Bethesda, MD) and segmented using a custom-made routine that incorporated the NIH Image commands *Threshold* and *Analyze Particles*. Threshold works by segmenting the beads from the background based on the intensity values. Analyze Particles detects the center of each particle by tracing the edge of each bead and computing its centroid.[35–37] To identify each particle and generate its trajectory, the positions of the beads were matched frame by frame, using a custom-made routine incorporated into NIH Image. Frame-by-frame matching assumes that the closest particle in the next frame is the same particle, which is a reasonable assumption because the change in position from frame to frame was very small compared to the spacing between beads.[34] Spatial resolution was assessed by fixing microspheres, using a strong adhesive (Loctite, Newington, CT), to the coverslip and measuring their apparent displacement. These displacements did not exceed ≈5 nm over 20 min, which we took as our higher limit of resolution for measured displacements.[34]

J. Measurement of the magnetic-tweezing force acting on the microsphere

A schematic of the forces acting on a magnetic bead, which is attached to a DNA molecule, is shown in Fig. 9. A lateral magnetic force, F_M, causes a displacement in the position of the bead, which produces an extension, x in the DNA. The resulting tension in the DNA chain, F_{Ext}, stretches the molecule to a new size, $L_0 = l_0 + x$, where l_0 is the initial length of the DNA molecule. This stretching force as well as the extension are obtained by solving the system of equations obtained from force balances in the horizontal and vertical directions at equilibrium

$$F_M = F_{\mathrm{Ext}} \sin\theta \quad \text{and,} \tag{5}$$

$$mg = F_{\mathrm{Ext}} \cos\theta, \tag{6}$$

where the mass m is the product of the bead volume by the density difference of the bead and the buffer solution. Here

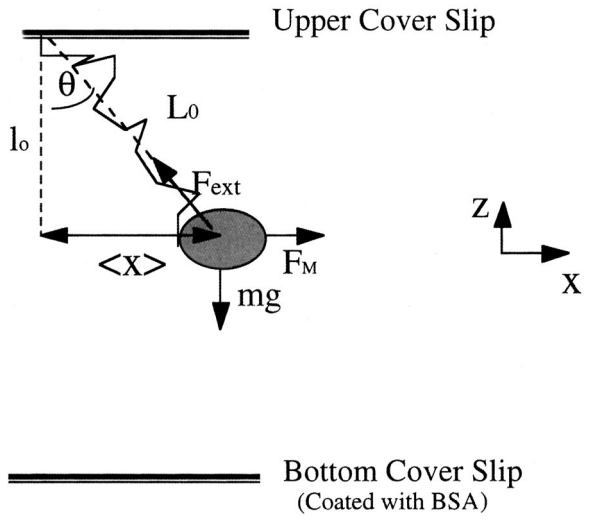

FIG. 9. Schematic of the forces acting on a magnetic bead, which is attached to a DNA molecule. A lateral magnetic force, F_M, causes a displacement in the position of the bead, which produces an extension, x in the DNA. The resulting tension in the DNA chain, F_{Ext}, stretches the molecule to a new size, $L_0 = l_0 + x$, where l_0 is the initial length of the DNA molecule. This stretching force as well as the extension are obtained by solving the system of equations obtained from force balances in the horizontal and vertical directions at equilibrium.

$$\sin\theta = \frac{\langle x\rangle}{L_0}, \tag{7}$$

where $\langle x\rangle$ is the time-average position of the bead. We square Eqs. (5) and (6) and add the results

$$F_{\mathrm{Ext}} = \sqrt{F_M^2 + (mg)^2}. \tag{8}$$

The total extension of DNA, L_0, is determined from Eqs. (5), (7), and (8)

$$L_0 = \frac{\sqrt{F_M^2 + (mg)^2}}{F_M}\langle x\rangle \quad \text{or} \quad L_0 = \sqrt{\langle x\rangle^2 + l_0^2}. \tag{9}$$

The extension $\langle x\rangle$ of the ''blob'' formed by the DNA molecule is measured as a function of the stretching force F_{ext}, which is related to the force F_M produced by the magnetic tweezers via Eq. (8).

The function generator (Stanford Research Scientific, Palo Alto, CA) sends a signal simultaneously to an oscilloscope and to the Sorensen power supply (see above), which in turn transforms the signal into current. After setting the current in the homogeneous coils at 2 A, we applied a step function of increasing magnitudes to the gradient coil. The output voltage of the oscilloscope was recorded, and the magnetic bead velocity is computed. The calibration curve converting the oscilloscope voltage readings (see Fig. 5) to force values was displayed in Fig. 7. For gradient voltages greater than 1750 mV corresponding to a gradient coil current of ≈6 A, the force reached a plateau as the homogeneous current at the center was not high enough to offset the gradient. Consequently, one had to increase the homogeneous current and repeat the experiments by varying the gradient current. Most importantly, the forces changed linearly with the voltage signals. The highest resolution of the Sorensen power supply providing the gradient current is 2 mV; at this current, the force generated on a 2.8-μm-diam bead was ≈0.1 pN.

F_{ext} and $\langle x\rangle$ values were used to generate the force-extension curve. A nonlinear least-square fit macro of the wormlike-chain equation was used to extract the contour length L_0 and the persistence length ξ of the DNA molecule.[38]

IV. RESULTS AND DISCUSSION

The physical and biochemical properties of individual biopolymers have been probed using an array of instruments such as glass needles,[39,40] hydrodynamic flows,[32,41] electric-field gradients,[42] micropipette aspiration,[43,44] optical tweezers,[45–50] and AFM.[28,51–53] Here, we measured the micromechanical properties of a single λ-phage DNA molecule using highly uniform magnetic tweezers and end attachment to a primer-grafted glass coverslip.

The homogeneity of the magnetic-field gradient was required to apply forces of constant magnitudes over large distances (see Sec. II). Our design allowed us to generate magnetic-field gradients as high as 100 T/m for a 1.5 cm gap size and 40 T/m for a 2 cm gap size (as measured using a magnetometer, see Fig. 7). Large gaps were required to allow the use of oil-immersion and water-immersion lenses, which are relatively wide, to come into contact with the glass coverslip (Fig. 1). Given the saturated magnetic moment of $1.42\times10^{-13}\,\mathrm{Am}^2$ and the magnetic-field gradient shown in Fig. 7 (≈3.8 T/m), one can estimate the force applied to the magnetic bead. In these conditions, the force is approximately $1.42\times3.8\times10^{-1}\approx0.5\,\mathrm{pN}$ [see Eq. (2)], which is within the range of measured forces (Fig. 11). Differences between measured and calculated forces stem from the assumption underlying Eq. (2), which ignores edge effects and field dispersion. Off-axis components of the magnetic force field were immediately detected by tracking the movement of unattached beads during the calibration. When required, the sets of homogeneous and gradient were realigned to minimize bead drift. In normal operating mode, drift of the bead tested over large distances were undetectable.

The DNA attachment procedure involved many steps: from the glass coverslip to the bifunctional cross-linker, to the 12 bp primer, to the λ-phage DNA molecule, to a biotin molecule, to the streptavidin-coated superparamagnetic bead. To ensure the viability of the overall procedure, each step described in the surface-modification section was tested using fluorescent microscopy or spectrophotometry. A challenge that we encountered was the fact that beads adhered easily to the lower coverslip surface in the chamber. Using an extra force along the optical axis or increasing the solution density to match the bead density did not constitute satisfactory solutions. The DNA molecules were instead end attached to the upper coverslip of the flow chamber (Fig. 9). This solution was the most warranted as we could use physiological buffers (no need for density matching) and avoided the cumbersome calibration of a z-axis manipulator. We verified that DNA molecules were successfully hung from the top plate of the microscope chamber by monitoring thermal

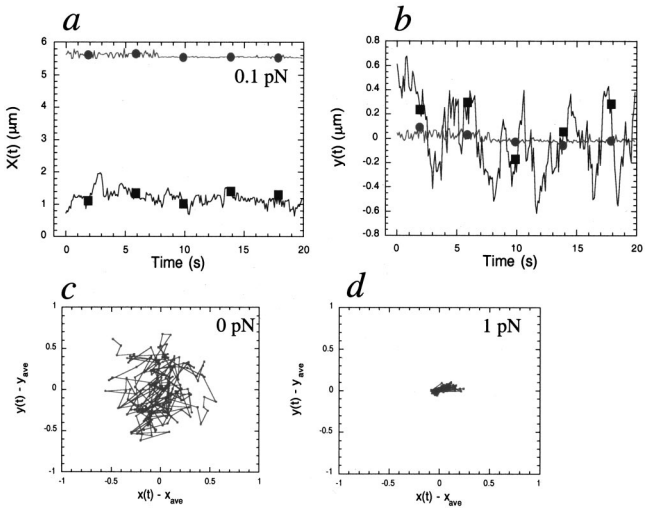

FIG. 10. Displacements of a magnetic bead end tethered to a DNA molecule in the presence and absence of an external magnetic force. Time-dependent displacements of the DNA-tethered bead (a) along the axis of the magnetic coils (x axis) and (b) normal to that axis in the plane normal to the optical axis (y axis) when the bead is subject to a zero (■) and a 0.1 pN (●) force. (c) Time-dependent x-y displacements of a DNA-tethered bead in the absence of the force field, and (d) subject to a 0.1 pN force. In (c) and (d), time-dependent coordinates $x(t)$ and $y(t)$ of the bead were translated by the time-averaged projections of the bead position, x_{ave} and y_{ave}. Displacements are in μm.

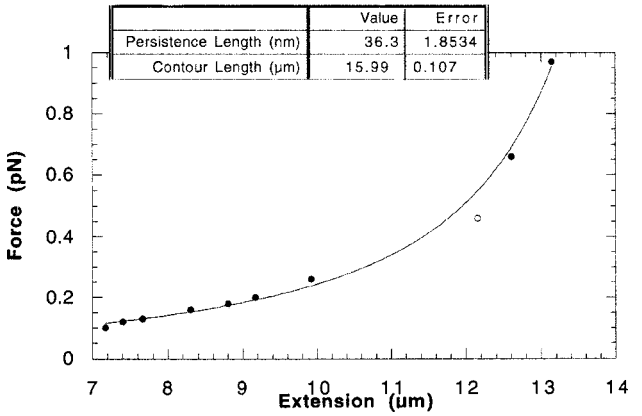

FIG. 11. Force-extension curve for a single λ-phage DNA molecule. Contour length and persistence length of λ-phage DNA are extracted using the worm-like-chain model.

displacements of the magnetic bead. Displacements of the end-attached beads were easily distinguished from those from the beads end-nonspecifically bound to the lower coverslip by changing the focal plane of observation. The attachment of the DNA molecule to the superparamagnetic bead was verified by fluorescently labeling both the DNA molecule and the bead for light-microscopy observations.[3]

After successful end attachment of the DNA molecule to both the flow chamber's top plate and the magnetic bead, the DNA molecule was subjected to increasing magnetic forces. For each force amplitude and to reduce the error on the measured DNA extension, the force was reversed and the position of the bead was measured. In the absence of an external magnetic field, the bead underwent Brownian motion (Fig. 10). For each new amplitude, the bead moved into a new location where it adopted a restricted Brownian motion (Fig. 10). Using our particle tracking software, the new location was recorded as a function of the applied voltage.

High DNA grafting densities on beads may lead to complex, seemingly irreproducible force-extension curves. We attributed the erratic behavior occasionally observed in our measurements to multiple DNA attachments to a single bead, or to supercoiled or nicked DNA. For instance, the number of molecules being stretched could be inferred from the measured persistence length (see below). A two-molecule system was twice as stiff as a single-molecule attachment. Consequently, the persistence length of the former was half that of the latter.

By plotting the values of F_{Ext} and L_0 derived from Eqs. 8 and 9, the data were fit with the WLC model and values of the contour length and persistence length of a single λ-phage DNA molecule were extracted (Fig. 11).[54] We determined the contour length of the λ-phage DNA to be $L \approx 16.0 \pm 0.1\ \mu$m and the persistence length to be $\xi \approx 36 \pm 2$ nm. The contour length was in reasonable agreement with the theoretical length of λ-phage DNA, $\approx 16.5\ \mu$m ($\approx 48\,502$ bp $\times 0.34$ nm/bp). The measured persistence length was also in good agreement with those reported by other research groups: $\xi \approx 53$ nm in 10 mM Na^+,[38] ≈ 43 nm in 93 mM Na^+,[55] and ≈ 15 nm in 80 mM Na^+.[56]

Single-DNA manipulation using magnetic tweezers offers a powerful approach for the study of the interactions between DNA and DNA-binding proteins. Using magnetic tweezers, the persistence length, and therefore the bending rigidity, of a DNA molecule can be measured before and after contact with a DNA-binding protein or upon binding of an enzyme. The cell utilizes many types of proteins, including histones, TATA-box binding proteins, and apparently the elastic protein titin[57,58] to locally bend and condense DNA. Magnetic tweezers can be used to evaluate binding cooperativity of these proteins when DNA is under tension.

ACKNOWLEDGMENTS

The authors thank Zina Meriden, Sami Alom Ruiz, Joshua Apgar, Jim Harden, Scot C. Kuo, Steve B. Smith, and Terrance Strick. D. W. acknowledges financial support from the National Science Foundation (DMR9623972).

[1] F. H. C. Crick and A. F. W. Hughes, Exp. Cell Res. **1**, 37 (1950).
[2] S. B. Smith, L. Finzi, and C. Bustamante, Science **258**, 1122 (1992).
[3] D. Wirtz, Phys. Rev. Lett. **75**, 2436 (1995).
[4] G. Uchida *et al.*, J. Phys. Soc. Jpn., 345 (1998).
[5] T. R. Strick *et al.*, J. Stat. Phys. **93**, 647 (1998).
[6] J. F. Leger *et al.*, Phys. Rev. Lett. **83**, 1066 (1999).
[7] M. Guthold *et al.*, Surf. Interface Anal. **27**, 437 (1999).
[8] M. D. Wang, Curr. Opin. Biotech. **10**, 81 (1999).
[9] N. Wang, J. P. Butler, and D. E. Ingber, Science **260**, 1124 (1993).
[10] F. Zienmann, J. Radler, and E. Sackmann, Biophys. J. **66**, 2210 (1994).
[11] F. Amblard *et al.*, Rev. Sci. Instrum. **67**, 818 (1996).
[12] M. Thie *et al.*, Mol. Hum. Repr. **3**, 275 (1997).
[13] F. Amblard *et al.*, Phys. Rev. Lett. **77**, 4470 (1997).
[14] N. Wang, Hypertension **32**, 162 (1998).
[15] M. Glogauer *et al.*, J. Biol. Chem. **273**, 1689 (1998).
[16] M. Glogauer and J. Ferrier, Pflug. Arch. Eur. J. Phys. **435**, 320 (1998).
[17] A. M. Lew, M. Glogauer, and C. A. G. McCulloch, Biochem. J. **341**, 647 (1999).
[18] A. R. Bausch, W. Môller, and E. Sackmann, Biophys. J. **76**, 573 (1999).

[19] T. R. Strick *et al.*, Biophys. J. **74**, 2016 (1998).
[20] F. G. Schmidt, F. Ziemann, and E. Sackmann, Eur. Biophys. J. **24**, 348 (1996).
[21] Y. Liu *et al.*, Biophys. J. **68**, 2137 (1995).
[22] V. Bangert and P. Mansfield, J. Phys. E **15**, 235 (1982).
[23] J. E. Tanner, Rev. Sci. Instrum. **36**, 1086 (1965).
[24] H. Saint-Jalmes, J. Taquin, and Y. Barjhoux, Magn. Reson. Med. **2**, 242 (1985).
[25] B. Alberts *et al.*, *Molecular Biology of the Cell* (Garland, 1994).
[26] C. Haber and D. Wirtz, Biophys. J. **79**, 1530 (2000).
[27] T. G. Mason, A. Dhople, and D. Wirtz, Macromolecules **31**, 3600 (1998).
[28] M. Hegner, S. B. Smith, and C. Bustamante, Proc. Natl. Acad. Sci. U.S.A. **96**, 10109 (1999).
[29] L. Ma *et al.*, J. Biol. Chem. **274**, 19145 (1999).
[30] A. Palmer *et al.*, Biophys. J. **76**, 1063 (1999).
[31] A. S. Silva *et al.*, Phys. Rev. E **54**, 5502 (1996).
[32] P. Leduc *et al.*, Nature (London) **399**, 564 (1999).
[33] C. Haber, S. Alom-Ruiz, and D. Wirtz, Proc. Natl. Acad. Sci. USA **97**, 10 792 (2000).
[34] J. Apgar *et al.*, Biophys. J. **79**, 1095 (2000).
[35] S. Yamada, D. Wirtz, and S. C. Kuo, Biophys. J. **78**, 1736 (2000).
[36] T. G. Mason *et al.*, Phys. Rev. Lett. **79**, 3282 (1997).
[37] T. G. Mason, A. Dhople, and D. Wirtz, in *Statistical Mechanics in Physics and Biology*, edited by D. Wirtz and T. C. Halsey (1997), Vol. 463, pp. 153–158.
[38] C. Bustamante *et al.*, Science **265**, 1599 (1994).
[39] A. Kishino and T. Yanagida, Nature (London) **334**, 74 (1988).
[40] R. B. Nicklas, Science **275**, 632 (1997).
[41] D. E. Smith and S. Chu, Science **281**, 1335 (1998).
[42] J. M. Schurr and S. B. Smith, Biopolymers **29**, 1161 (1990).
[43] E. A. Evans, Biophys. J. **30**, 265 (1980).
[44] V. Heinrich and E. Waugh, Ann. Biomed. Eng. **24**, 595 (1996).
[45] S. Kuo and N. P. Sheetz, Science **260**, 232 (1993).
[46] J. T. Finer, R. M. Simmons, and J. A. Spudich, Nature (London) **368**, 113 (1994).
[47] T. T. Perkins *et al.*, Science **264**, 822 (1994).
[48] K. Svoboda and S. M. Block, Annu. Rev. Biophys. Biomol. Struct. **23**, 247 (1994).
[49] M. D. Wang *et al.*, Biophys. J. **72**, 1335 (1997).
[50] M. S. Z. Kellermayer *et al.*, Science **276**, 1112 (1997).
[51] J. Yang, K. Takeyasu, and Z. Shao, FEBS Lett. **301**, 173 (1992).
[52] H. G. Hansma and D. E. Laney, Biophys. J. **70**, 1933 (1996).
[53] M. Rief *et al.*, Science **276**, 1109 (1997).
[54] C. Bouchiat *et al.*, Biophys. J. **76**, 409 (1998).
[55] C. G. Baumann *et al.*, Proc. Natl. Acad. Sci. U.S.A. **94**, 6185 (1997).
[56] P. Cluzel *et al.*, Science **271**, 792 (1996).
[57] J. L. Kim, D. B. Nikolov, and S. K. Burley, Nature (London) **365**, 520 (1993).
[58] C. Machado, C. E. Sunkel, and D. J. Andrew, J. Cell Biol. **141**, 321 (1998).